ickeds '04

International Conference
on Knowledge Engineering
and Decision Support

PROCEEDINGS

PORTO [PORTUGAL] 21 to 23 JULY 2004

+ INFO. > www.gecad.isep.ipp.pt/ICKEDS04

Application of Fractional Calculus in the System Modelling and Control

J. A. Tenreiro Machado, Ramiro S. Barbosa, Manuel F. Silva, Lino M. Figueiredo, Isabel S. Jesus, Alexandra F. Galhano

GRIS – Group of Robotics and Intelligent Systems
Department of Electrical Engineering, Institute of Engineering of Porto
Rua Dr. António Bernardino de Almeida, 4200-072 Porto, Portugal
{jtm,rbarbosa,mfsilva,lino,isj,afg}@dee.isep.ipp.pt

Abstract – Fractional Calculus (*FC*) goes back to the beginning of the theory of differential calculus. Nevertheless, the application of *FC* just emerged in the last two decades, due to the progress in the area of chaos that revealed subtle relationships with the *FC* concepts. In the field of dynamical systems theory some work has been carried out but the proposed models and algorithms are still in a preliminary stage of establishment. Having these ideas in mind, the paper discusses a *FC* perspective in the study of the dynamics and control of several systems.

Keywords: Fractional Calculus, Control, Modelling, Dynamical Systems.

I. INTRODUCTION

The generalization of the concept of derivative $D^{\alpha}[f(x)]$ to non-integer values of α goes back to the beginning of the theory of differential calculus. In fact, Leibniz, in his correspondence with Bernoulli, L'Hôpital and Wallis (1695), had several notes about the calculation of $D^{1/2}[f(x)]$. Nevertheless, the development of the theory of Fractional Calculus (*FC*) is due to the contributions of many mathematicians such as Euler, Liouville, Riemann and Letnikov [1-3]. The adoption of the *FC* in control algorithms has been recently studied using the frequency and discrete-time domains [4,5]. Nevertheless, this research is still giving its first steps and further investigation is required.

This article presents novel results on the dynamics and control of several distinct systems [6-8]. In this perspective, the paper is organized as follows. Section 2 presents the main mathematical aspects of the theory of fractional calculus and section 3 presents several case studies on the implementation of *FC*-based models and control systems. Finally, section 4 draws the main conclusions.

II. THEORY OF FRACTIONAL CALCULUS

A. Main Mathematical Aspects

Since the foundation of the differential calculus the generalization of the concept of derivative and integral to a non-integer order α has been the subject of several approaches. Due to this reason there are various definitions of fractional-order integrals (Table I) which are proved to be equivalent. Based on the proposed definitions it is possible to calculate the fractional-order integrals/derivatives of several functions (Table II). Nevertheless, the problem of devising and implementing fractional-order algorithms is not trivial and will be the matter of the next sections.

Table I- Some Definitions of Fractional-Order Integrals

Riemann-Liouville	$\left(I_{a+}^{\alpha}\varphi\right)(x)=\frac{1}{\Gamma(\alpha)}\int_a^x\frac{\varphi(t)}{(x-t)^{1-\alpha}}dt,\ a<x$
	$\left(D_{a+}^{\alpha}\varphi\right)(x)=\frac{1}{\Gamma(1-\alpha)}\frac{d}{dx}\int_a^x\frac{\varphi(t)}{(x-t)^{\alpha}}dt,\ a<x$
Grünwald-Letnikov	$\left(I_{a+}^{\alpha}\varphi\right)(x)=\frac{1}{\Gamma(\alpha)}\lim_{h\to+0}\left[h^{\alpha}\sum_{j=0}^{[(x-a)/h]}\frac{\Gamma(\alpha+j)}{\Gamma(j+1)}\varphi(x-jh)\right]$
Laplace	$L\left\{I_{0+}^{\alpha}\varphi\right\}=L\{\varphi\}/s^{\alpha},\ \mathrm{Re}(\alpha)>0$
	$L\left\{D_{0+}^{\alpha}\varphi\right\}=s^{\alpha}L\{\varphi\},\ \mathrm{Re}(\alpha)\geq 0$

Table II- Fractional-Order Integrals of Several Functions

$\varphi(x),\ x\in\Re$	$\left(I_{+}^{\alpha}\varphi\right)(x),\ x\in\Re,\ \alpha\in C$
$(x-a)^{\beta-1}$	$\frac{\Gamma(\beta)}{\Gamma(\alpha+\beta)}(x-a)^{\alpha+\beta-1},\ \mathrm{Re}(\beta)>0$
$e^{\lambda x}$	$\lambda^{-\alpha}e^{\lambda x},\ \mathrm{Re}(\lambda)>0$
$\begin{cases}\sin(\lambda x)\\ \cos(\lambda x)\end{cases}$	$\lambda^{-\alpha}\begin{cases}\sin(\lambda x-\alpha\pi/2)\\ \cos(\lambda x-\alpha\pi/2)\end{cases},\ \lambda>0,\ \mathrm{Re}(\alpha)>1$
$e^{\lambda x}\begin{cases}\sin(\gamma x)\\ \cos(\gamma x)\end{cases}$	$\frac{e^{\lambda x}}{(\lambda^2+\gamma^2)^{\alpha/2}}\begin{cases}\sin(\gamma x-\alpha\phi)\\ \cos(\gamma x-\alpha\phi)\end{cases},\ \phi=\arctan(\gamma/\lambda)$, $\gamma>0,\ \mathrm{Re}(\lambda)>1$

B. Approximations to Fractional-Order Derivatives

In this section we analyze two methods for implementing fractional-order derivatives, namely the frequency-based and the discrete-time approaches, and its implication in control algorithms.

In order to analyze a frequency-based approach to D^{α}, $0<\alpha<1$, let us consider the recursive circuit represented on Figure 1 such that:

$$I=\sum_{i=0}^{n}I_i,\ R_{i+1}=\frac{R_i}{\varepsilon},\ C_{i+1}=\frac{C_i}{\eta} \tag{1}$$

where η and ε are scale factors, I is the current due to an applied voltage V and R_i and C_i are the resistance and capacitance elements of the i^{th} branch of the circuit.

The admittance $Y(j\omega)$ is given by:

$$Y(j\omega)=\frac{I(j\omega)}{V(j\omega)}=\sum_{i=0}^{n}\frac{j\omega C\varepsilon^i}{j\omega CR+(\eta\varepsilon)^i} \tag{2}$$

Figure 2 shows the asymptotic Bode diagram of amplitude of $Y(j\omega)$. The pole and zero frequencies (ω_i

and ω_i') obey the recursive relationships:

$$\frac{\omega_{i+1}'}{\omega_i'} = \frac{\omega_{i+1}}{\omega_i} = \varepsilon\eta\,,\ \frac{\omega_i}{\omega_i'} = \varepsilon\,,\ \frac{\omega_{i+1}'}{\omega_i} = \eta \tag{3}$$

From the Bode diagram of amplitude or of phase, the average slope m' can be calculated as:

$$m' = \frac{\log\varepsilon}{\log\varepsilon + \log\eta} \tag{4}$$

Consequently, the circuit of Figure 1 represents an approach to D^{α}, $0 < \alpha < 1$, with $m' = \alpha$, based on a recursive pole/zero placement in the frequency domain.

As mentioned in section II, the Laplace definition for a derivative of order $\alpha \in C$ is a 'direct' generalization of the classical integer-order scheme with the multiplication of the signal transform by the *s* operator. Therefore, in what concerns automatic control theory this means that frequency-based analysis methods have a straightforward adaptation to their fractional-order counterparts. Nevertheless, the implementation based on the Laplace definition (adopting the frequency domain) requires an infinite number of poles and zeros obeying a recursive relationship [4]. In a real approximation the finite number of poles and zeros yields a ripple in the frequency response and a limited bandwidth.

The mathematical definition of a derivative of fractional order has been the subject of several different approaches [1]. For example, Eq. (5) and Eq. (6), represent the Laplace (for zero initial conditions) and the Grünwald-Letnikov definitions of the fractional derivative of order α of the signal $x(t)$:

$$D^{\alpha}[x(t)] = L^{-1}\{s^{\alpha}\,X(s)\} \tag{5}$$

$$D^{\alpha}x(t) = \lim_{h\to 0}\left[\frac{1}{h^{\alpha}}\sum_{k=0}^{\infty}(-1)^k\frac{\Gamma(\alpha+1)}{\Gamma(k+1)\Gamma(\alpha-k+1)}x(t-kh)\right] \tag{6}$$

where Γ is the gamma function and h is the time increment. This formulation [5] inspired a discrete-time calculation algorithm, based on the approximation of the time increment h through the sampling period T, yielding the equation in the z domain:

$$\frac{Z\{D^{\alpha}x(t)\}}{X(z)} \approx \frac{1}{T^{\alpha}}\sum_{k=0}^{\infty}\frac{(-1)^k\,\Gamma(\alpha+1)}{k!\;\Gamma(\alpha-k+1)}z^{-k} = \left(\frac{1-z^{-1}}{T}\right)^{\alpha} \tag{7}$$

An implementation of (7) corresponds to a *r*-term truncated series or to a Padé fraction.

An important aspect of fractional-order controllers can be illustrated through the elemental control system represented in Figure 3, with open-loop transfer function $G(s) = Ks^{-\alpha}$ $(1 < \alpha < 2)$ in the forward path. The open-loop Bode diagrams (Figure 4) of amplitude and phase have a slope of -20α *dB*/*dec* and a constant phase of $-\alpha\pi/2$ *rad*, respectively. Therefore, the closed-loop system has a constant phase margin of $\pi(1-\alpha/2)$ *rad* that is independent of the system gain *K*.

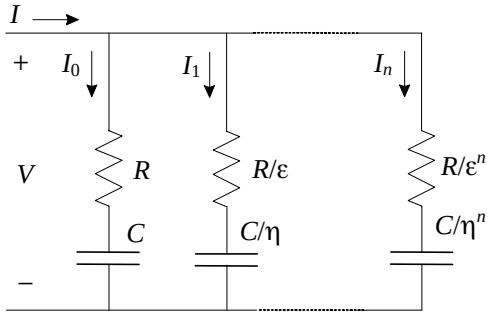

Figure 1- Electrical circuit with a recursive association of resistance and capacitance elements.

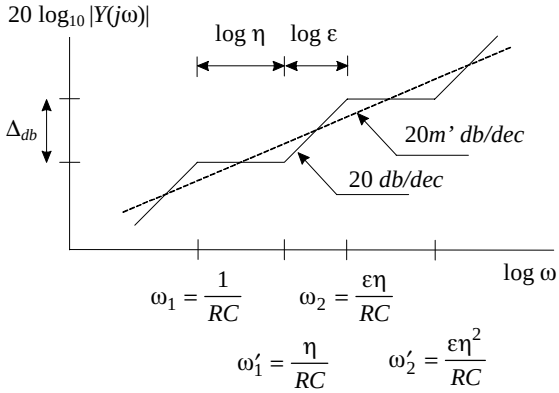

Figure 2- Bode diagrams of amplitude of $Y(j\omega)$.

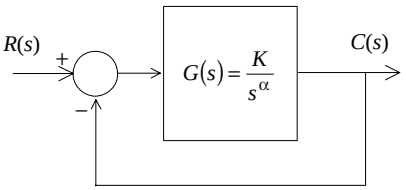

Figure 3- Block diagram for an elemental feedback control system of fractional order α.

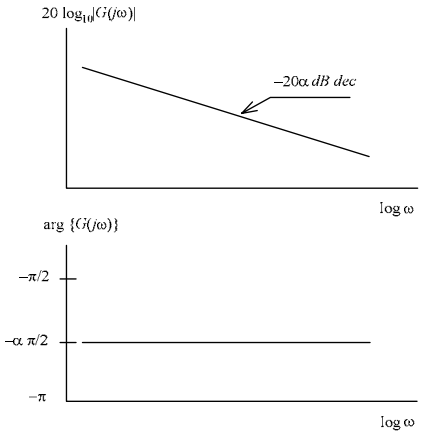

Figure 4- Open-loop Bode diagrams of amplitude and phase for a system of fractional order $1 < \alpha < 2$.

III. CASE STUDIES

In this section we analyse the modelling and control of several systems based on the theory of fractional calculus.

A. Controller Tuning Based on Fractional-Order Systems Theory

PID controllers are the most commonly used control algorithms in industry. Along the last decades were developed many tuning techniques for the determination of the *PID* parameters. Among them, the most well known are the Ziegler-Nichols tuning rules. However, these heuristic rules do not produce satisfactory results giving very poor damping. Therefore, other methods were developed such as root-locus based techniques and methods based on optimization techniques.

In this section we present a new strategy for the tuning of *PID* controllers. The proposed method is known as reference model tuning and consists on the integral square error (*ISE*) minimization between the step responses of a desired fractional-order transfer function and the actual system with the *PID* controller. The reference model is represented as an ideal closed-loop system whose open-loop is the Bode's ideal transfer function, which has the form:

$$L(s) = \left(\frac{\omega_c}{s}\right)^{\gamma}, \quad (\gamma \in \mathbb{R}) \tag{8}$$

where ω_c is the gain crossover frequency, that is $|L(j\omega_c)| = 1$. The parameter γ is the slope of magnitude curve, on a log-log scale, and may assume integer as well as noninteger values. In fact, the transfer function (8) is a fractional-order differentiator for $\gamma < 0$ and a fractional-order integrator for $\gamma > 0$.

Therefore, in this section we address the closed-loop system with Bode's ideal transfer function (8) as a reference system for the tuning of *PID* controllers [6]. For that purpose we consider the standard closed-loop system shown in Figure 5, where $G_c(s)$ and $G_p(s)$ are the controller and the plant transfer functions, respectively. The system may be subject for both setpoint and disturbance inputs, respectively $r(t)$ and $p(t)$.

The transfer function of a practical *PID* controller may assume the following form:

$$G_c(s) = \frac{U(s)}{E(s)} = K\left(1 + \frac{1}{T_i s} + \frac{sT_d}{1 + sT_d/N}\right) \tag{9}$$

where $U(s)$ and $E(s)$ denote the control and the error signals, respectively. The tuning parameters K, T_i, and T_d are correspondingly the proportional gain, the integral time constant and the derivative time constant. The derivative term of the *PID* controller (9) is implemented by a band-limited differentiator in order to reduce the control effort or any existent high frequency measurement noise. Usually $3 \le N \le 20$.

For the determination of the *PID* parameters (K, T_i, T_d) we consider the general tuning structure system represented in Figure 6. Note that this is a batch process.

The reference model is given by the transfer function of the closed-loop system with the Bode's ideal transfer function $L(s)$ of expression (8) and is represented in Figure 2 (with $K = \omega_c^{\gamma}$), yielding:

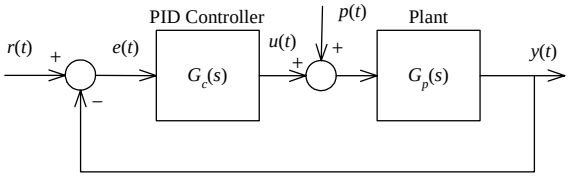

Figure 5- Block diagram of a feedback control system with *PID* controller $G_c(s)$.

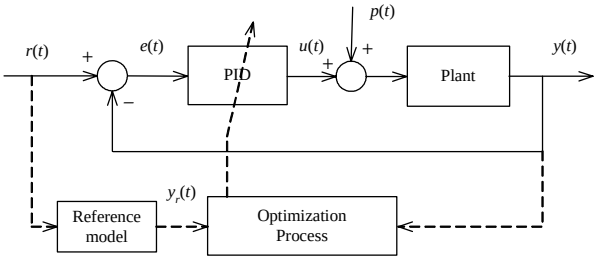

Figure 6- System structure for *PID* controller tuning.

$$G(s) = \frac{L(s)}{1 + L(s)} = \frac{1}{\left(s/\omega_c\right)^{\gamma} + 1}, \quad (\gamma \in \mathbb{R}^{+}) \tag{10}$$

where the parameters γ and ω_c denote the order and the crossover frequency, respectively. For the case under study, the order λ may assume real noninteger values such that $1 < \gamma < 2$ (*i.e.*, a fractional-order relaxation system). The main frequency characteristics of transfer function (10) are given in the previous section. The time response $y(t)$ to a unit step input is given by:

$$\begin{aligned} y(t) &= L^{-1}\left\{\frac{\omega_c^{\gamma}}{s(s^{\gamma} + \omega_c^{\gamma})}\right\} \\ &= 1 - \sum_{n=0}^{\infty} \frac{\left[-(\omega_c t)^{\gamma}\right]^n}{\Gamma(1 + \gamma n)} = 1 - E_{\gamma}\left[-(\omega_c t)^{\gamma}\right] \end{aligned} \tag{11}$$

where $E_\gamma(x)$ is the one-parameter Mittag-Leffler function. This function is a generalization of the common exponential function since for $\gamma = 1$ we have $E_1(x) = e^x$.

For the determination of the optimal *PID* settings we minimize the *ISE* of the resultant error function, $e(t) = y_r(t) - y(t)$. That is, the difference between the desired output response $y_r(t)$ produced by the reference model and the output response $y(t)$ of the closed loop system with the *PID* (Fig. 6). This optimization criterion is defined as:

$$J(K, T_i, T_d) = \int_0^{\infty} \left[y(t) - y_r(t)\right]^2 dt \tag{12}$$

where (K, T_i, T_d) are the controller parameters to be optimized. Thus, the tuning of the controller consists in finding the optimum parameters (K, T_i, T_d) that minimizes $J(K, T_i, T_d)$, while satisfying the stability of the closed-loop system and positive controller parameters.

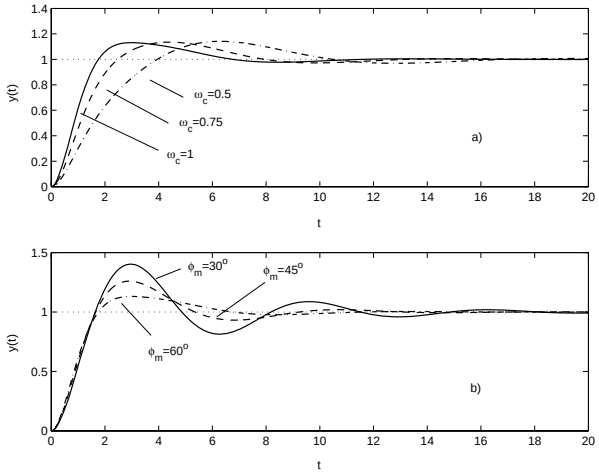

Figure 7- Step setpoint responses of the closed-loop system for $G_p(s)$: a) $\phi_m = 60^o$and $\omega_c = \{0.5, 0.75, 1.0\}$ rad/s; b) $\omega_c = 1.0$ rad/s and $\phi_m = \{30^o, 45^o, 60^o\}$.

To illustrate the proposed methodology we consider the example of a third-order plant transfer function:

$$G_p(s) = \frac{1}{(s+1)^3} \tag{13}$$

Figure 7 shows the step responses of the closed-loop system with the *PID* for the transfer function $G_p(s)$. In Figure 7a) is shown the evolution of the step responses as we vary the gain crossover frequency $\omega_c = \{0.5, 0.75, 1.0\}$ rad/s for a fixed value of the order (or phase margin) $\gamma = 4/3$ (or $\phi_m = 60^o$). Alternatively, Figure 7b) shows the step responses for $\phi_m = \{30^o, 45^o, 60^o\}$ and $\omega_c = 1$ rad/s. We observe that by varying the crossover frequency ω_c, while maintaining a fixed order γ, we get different rise times (*i.e.*, natural frequencies) of the output response with a constant overshoot *(i.e.*, an iso-damping system). On the other hand, for a fixed crossover frequency ω_c and by varying the order γ we get different overshoots of the output response with an almost constant rise time. Therefore, with the proposed method we can shape the output response, close to the desired response, by adjusting the tuning parameters (γ, ω_c) of the fractional reference model.

We test the method on several cases studies that revealed good results demonstrating its applicability. Furthermore, we compared with other tuning methods showing that we get comparable or superior results. The proposed methodology gives closed-loop systems robust to gain variations and step responses exhibiting an iso-damping property. It also proves that although the closed-loop system with the *PID* controller is treated as an integer-order system it can be analysed as fractional-order system and we can (and should) take advantage of that. This analysis may constitute a step towards the establishment of a common tuning scheme for integer-order and noninteger-order systems.

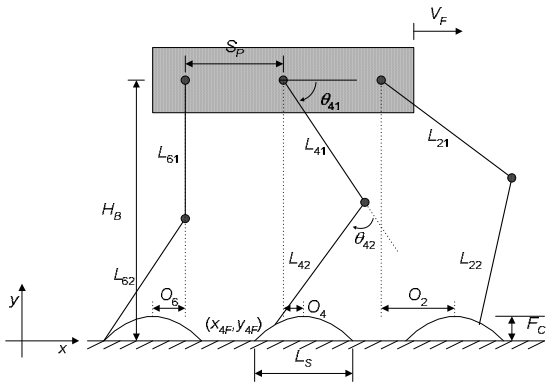

Figure 8- Coordinate system and variables that characterize the motion trajectories of the multi-legged robot.

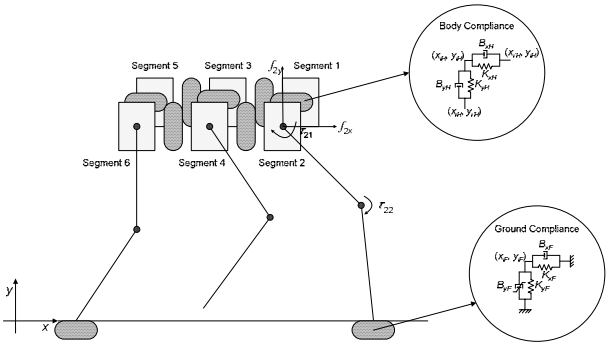

Figure 9- Model of the robot body and foot-ground interaction.

B. Fractional-Order Control of a Hexapod Robot

In this section we compare the performance of two robot leg controllers, namely Proportional and Derivative (*PD*) and Fractional-Order (*FO*) schemes, in the case of a hexapod robot with leg joints having viscous friction, flexibility and backlash and joint actuator saturation [7].

We consider a walking system (Figure 8) with six legs, equally distributed along both sides of the robot body, having each two rotational joints at the hip and knee.

Motion is described by means of a world coordinate system. The kinematic model comprises: the cycle time T, the duty factor β, the transference time $t_T = (1-\beta)T$, the support time $t_S = \beta T$, the step length L_S, the stroke pitch S_P, the body height H_B, the maximum foot clearance F_C, the i^{th} leg lengths L_{i1} and L_{i2} and the foot trajectory offset O_i ($i = 1, \ldots, n$). Moreover, we consider a periodic trajectory for each foot, with body velocity $V_F = L_S / T$. Based on this data, the trajectory generator is responsible for producing a motion that synchronises and coordinates the legs. Once defined the coordinates of the feet and hips of the robot it is possible to obtain the leg joint positions and velocities using the inverse kinematics $\boldsymbol{\psi}^{-1}$ and the Jacobian $\mathbf{J} = \partial\boldsymbol{\psi}/\partial\boldsymbol{\theta}$.

The dynamical model of the hexapod robot (Figure 9) addresses the foot-ground interaction, the body and the legs dynamics. The contact of the i^{th} robot feet with the ground is modelled through a non-linear system with damping $B_{i\eta}$ and stiffness $K_{i\eta}$ ($\eta = \{x, y\}$) in the {horizontal, vertical} directions, respectively.

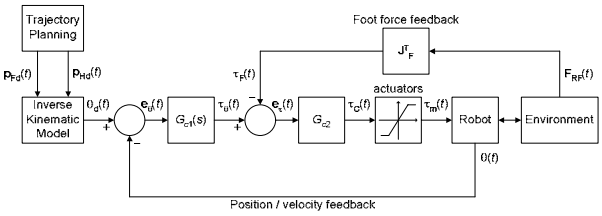

Figure 10- Hexapod robot control architecture.

Furthermore, the robot body is divided in *n* identical segments (each with mass $M_b n^{-1}$) and a linear spring-dashpot system is adopted to implement the intra-body compliance. The legs dynamics is modelled through the Lagrangian formalism.

We consider also that the joint actuators may saturate. Therefore, the motor effective torque is limited by the maximum torque that the actuator can supply, that is $\tau_{ijm} \leq \tau_{ijMax}$.

The general control architecture of the hexapod robot is presented in Figure 10. For $G_{c1}(s)$ we adopt either an integer *PD* or a *FO* algorithm while for G_{c2} it is considered a simple *P* controller.

For the integer order *PD* algorithm we have:

$$G_{C1j}(s) = Kp_j + Kd_j s, \quad j = 1,2 \tag{14}$$

where Kp_j and Kd_j are the proportional and derivative gains.

For the *FO* algorithm we have:

$$G_{C1j}(s) = Kp_j + K_j s^{\alpha_j}, \quad -1 < \alpha_j < 1, \quad j = 1,2 \tag{15}$$

where Kp_j and K_j are gains and α_j is the fractional order.

For implementing the *FO* algorithm (Eq. (15)) it is adopted a discrete-time 4th-order Padé approximation (a_{ij}, $b_{ij} \in \Re$, j = 1,2) yielding an equation in the *z*-domain of the type:

$$G_{C1j}(z) \approx K_j \sum_{i=0}^{i=4} a_{ij} z^{-i} \Big/ \sum_{i=0}^{i=4} b_{ij} z^{-i} \tag{16}$$

where K_j is the controller gain.

We start by tuning the controllers, assuming that the robot actuators are almost ideal (τ_{ijMax} = 400 Nm) and the leg joints are ideal. To tune the controller parameters we adopt a systematic method, testing and evaluating several possible combinations of controller parameters, for both control architectures, while establishing a compromise in what concerns the minimisation of the hips trajectories errors and joint torques.

With these controller settings, we analyze the system performance for the three different dynamical effects on the leg joints. We start by considering an ideal joint transmission and, afterwards, we augment the model by including viscous friction, flexibility and backlash. Furthermore, we consider the *PD* controller and different values of τ_{ijMax}, in order to observe its influence upon the locomotion and, in a second phase, we repeat the experiments for the case of a *FO* controller.

For the ideal transmission we conclude that neither the hips trajectories errors nor the joint torques present

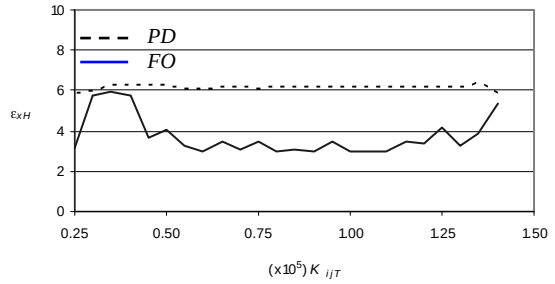

Figure 11- Plots of the hip trajectory error *vs.* K_{ijT} for the *PD* and *FO* controllers, with τ_{ijMax} = 100 Nm.

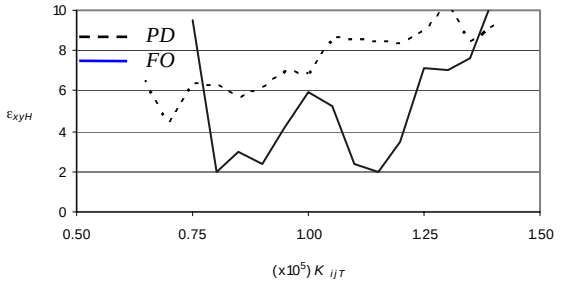

Figure 12- Plots of the hip trajectory error *vs.* K_{ijT} for the *PD* and *FO* controllers, with τ_{ijMax} = 100 Nm.

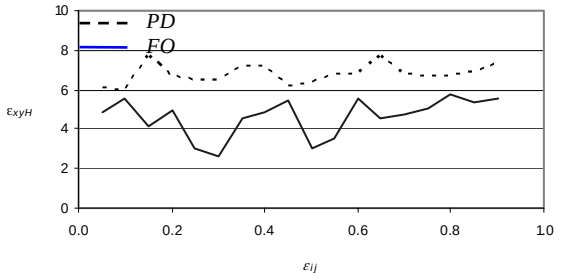

Figure 13- Plots of the hip trajectory error *vs.* ε_{ij} for the *PD* and *FO* controllers, with τ_{ijMax} = 100 Nm.

significant variation for moderate saturation levels (*e.g.*, τ_{Max} > 120 Nm) being the performance of both controllers approximately similar. In the case of strong actuator saturation (*e.g.*, τ_{Max} < 100 Nm) both the hips trajectories errors and the joint torques present reveal a large degradation with difficulties both for the *PD* and the *FO* algorithms. Nevertheless, this situation is not realistic since it corresponds to operating conditions requiring joint torques much higher than those established by the saturation level. On the other hand, as expected, the robot hips trajectories errors are higher the smaller the maximum actuator torque.

The second situation consists of actuator model with viscous friction and joint transmission with flexibility. For this case the *FO* controller presents the lower values for the hips trajectories errors (Figure 11) and the joint torques (along most of the range of variation of K_{ijT} that keeps the robot locomotion stable) being the effect more noticeable the smaller the values of τ_{ijMax}.

On a third set of experiments we consider that the joint transmission model includes viscous friction, flexibility and backlash.

For this case, the *FO* controller presents also lower values for the hips trajectories errors and the joint torques than the *PD* controller. This effect is more pronounced for smaller values of τ_{ijMax} and is visible on a large range of variation of the flexibility K_{ijT}, that keep the robot locomotion stable, as can be seen in Figure 12.

The same conclusion is valid for the entire range of variation of the restitution coefficient ε_{ij} (Figure 13) and on a large range of variation of the backlash width h_{ij}. The charts of the joint torques are very similar to those of the hips trajectories errors, for the entire ranges of variation of ε_{ij} and h_{ij}, and consequently not presented here.

These experiments reveal that the *FO* controller presents superior results than the *PD* algorithm when we have actuator saturation and dynamical phenomena on the joints. This means that, although tuned for identical performance in an ideal situation, the *FO* algorithm is more robust in a real operating condition.

C. Simulation and Dynamical Analysis of Freeway Traffic Systems

In order to study the dynamics of traffic systems it was developed the Simulator of Intelligent Transportation Systems (*SITS*). *SITS* is a software tool based on a microscopic simulation approach, which reproduces real traffic conditions in an urban or non-urban network. The program provides a detailed modelling of the traffic network, distinguishing between different types of vehicles and drivers and considering a wide range of network geometries. *SITS* uses a flexible structure that allows the integration of simulation facilities for any of the *ITS* related areas. This new simulation package is an object-oriented implementation written in C++ for MsWindows. The overall model structure is represented on Figure 14.

SITS models each vehicle as a separate entity in the network according to the state diagram showing in Figure 15. Therefore, are defined five states {1-aceleration, 2-braking, 3-cruise speed, 4-stopped, 5-collision} that represent the possible vehicle states in a traffic systems.

In this modelling structure, so called State-Oriented Modelling (*SOM*), every single vehicle in the network has one possible state for each sampling period. The transition between each state depends on the driver behaviour model and its surrounding environment. Some transitions are not possible; for instance, it is not possible to move from state #4 (stopped) to state #2 (braking), although it is possible to move from state #2 to state #4.

A set of simulation experiments are developed in order to estimate the influence of the vehicle speed $v(t;x)$, the road length l and the number of lanes n_l in the traffic flow $\phi(t;x)$ at time t and road coordinate x. For a road with n_l lanes the Transfer Function (*TF*) between the flow measured by two sensors is calculated by the expression:

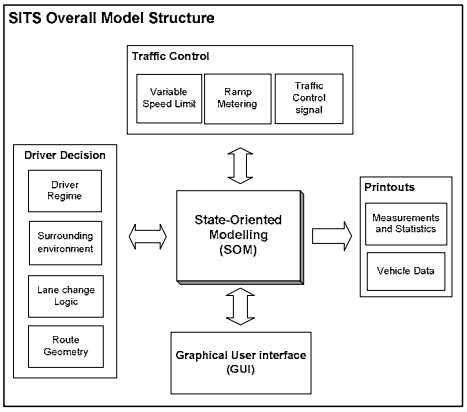

Figure 14- *SITS* overall model structure.

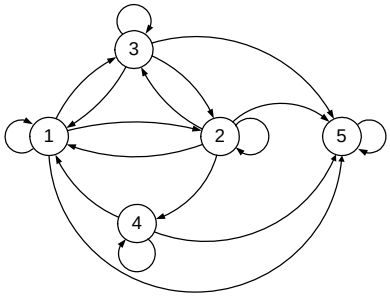

Figure 15- *SITS* state diagram (1-aceleration, 2-braking, 3-cruise speed, 4-stopped, 5-collision).

$$G_{r,k}(s; x_j, x_i) = \Phi_r(s;x_j)/\Phi_k(s;x_i) \quad (17)$$

where k, r = 1,2,…, n_l define the lane number and, x_i and x_j represent the road coordinates ($0 \le x_i \le x_j \le l$), respectively.

The first group of experiments considers a one-lane road (*i.e.*, $k = r = 1$) with length $l = 1000$ m. Across the road are placed n_s sensors equally spaced. The first sensor is placed at the beginning of the road (*i.e.*, at $x_i = 0$) and the last sensor at the end (*i.e.*, at $x_j = l$). Therefore, we calculate the *TF* between two traffic flows at the beginning and the end of the road such that, $\phi_1(t;0) \in [1, 8]$ vehicles s^{-1} for a vehicle speed $v_1(t;0) \in [30, 70]$ km h^{-1}, that is, for $v_1(t;0) \in [v_{av} - \Delta v, v_{av} + \Delta v]$, where $v_{av} = 50$ km h^{-1} is the average vehicle speed and $\Delta v = 20$ km h^{-1} is the maximum speed variation. These values are generated according to a uniform probability distribution function.

The results obtained of the polar plot for the *TF* $G_{1,1}(s;1000,0) = \Phi_1(s;1000)/\Phi_1(s;0)$ between the traffic flow at the beginning and end of the one-lane road is distinct from those usual in systems theory revealing a large variability. Moreover, due to the stochastic nature of the phenomena involved different experiments using the same input range parameters result in different *TF*s.

In fact traffic flow is a complex system but it was shown [8] that, by embedding statistics and Fourier transform (leading to the concept of Statistical Transfer Function (*STF*)), we could analyse the system dynamics in the perspective of systems theory.

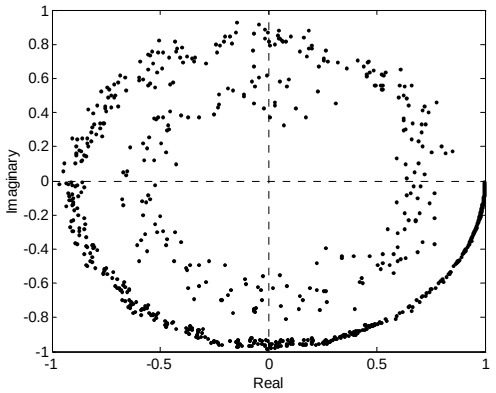

Figure 16- The *STF* $T_{1,1}(s;1000,0)$ for $n = 2000$ experiments with $\phi_1(t;0) \in [1, 8]$ vehicles s^{-1} and $v_1(t;0) \in [30, 70]$ km h^{-1} ($v_{av} = 50$ km h^{-1}, $\Delta v = 20$ km h^{-1}, $l = 1000$ m and $n_l = 1$).

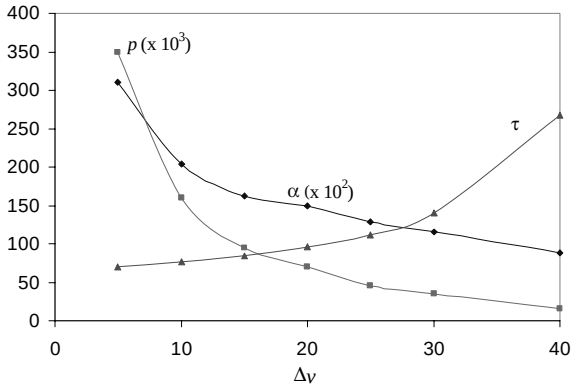

Figure 17- Time delay τ, pole p and fractional order α *versus* Δv for an average vehicle speed $v_{av} = 50$ km h^{-1}, $n_l = 1$, $l = 1000$ m and $\phi_1(t;0) \in [1, 8]$ vehicles s^{-1}.

To illustrate the proposed modelling concept (*STF*), the simulation was repeated for a sample of $n = 2000$ and it was observed the existence of a convergence of the *STF*, $T_{1,1}(s;1000,0)$, as show in Figure 16, for a one-lane road with length $l = 1000$ m $\phi_1(t;0) \in [1, 8]$ vehicles s^{-1} and $v_1(t;0) \in [30, 70]$ km h^{-1}.

Based on this result we can approximate numerically the *STF* to a fractional order system with time delay yielding the approximate expression

$$T_{1,1}(s;1000,0) = \frac{k_B \; e^{-\tau s}}{\left(\frac{s}{p}+1\right)^{\alpha}} \tag{18}$$

For the numerical parameters of Fig. 16 we get $k_B = 1.0$, $\tau = 96.0$ sec, $p = 0.07$ and $\alpha = 1.5$.

The parameters (τ, p, α) vary with the average speed v_{av} and its range of variation Δv, the road length l and the input vehicle flow ϕ_1. For example, Figure 17 shows (τ, p, α) versus Δv for $v_{av} = 50$ km h^{-1}.

It is interesting to note that (τ, p) $\rightarrow$ (∞, 0), when $\Delta v \rightarrow v_{av}$, and ($\tau$, p) $\rightarrow$ ($l\ v_{av}^{-1}$, ∞), when $\Delta v \rightarrow 0$.

These results are consistent with our experience that suggests a pure transport delay $T(s) \approx e^{-\tau s}$ ($\tau = l\ v_{av}^{-1}$), $\Delta v \rightarrow 0$ and $T(s) \approx 0$, when $\Delta v \rightarrow v_{av}$ (because of the existence of a blocking cars, with zero speed, on the road).

D. Heat Diffusion

In many industrial applications it is important that the temperature distribution in the work pieces should be as uniform as possible. It is clearly difficult to determine the temperature distribution in the interior of the material or system, but the measurement of the surface temperature is routine. Therefore, we encounter the problem of the observability and control of the temperature distribution throughout the material from the available surface measurements.

The heat diffusion is represented by a partial linear differential equation (*PDE*) [9]:

$$\frac{\partial u}{\partial t} = k\left(\frac{\partial^2 u}{\partial x^2} + \frac{\partial^2 u}{\partial y^2} + \frac{\partial^2 u}{\partial z^2}\right) \tag{19}$$

where k is the diffusivity, t is the time, u is the temperature and (x, y, z) are the space cartesian coordinates.

This system involves the integration of a *PDE* of parabolic type for which the standard theory of parabolic *PDE*s guarantees the existence of a unique solution.

For the case of a planar perfectly isolated surface we apply a constant temperature U_0 at $x = 0$ and we analyse the heat diffusion along horizontal coordinate x. The heat diffusion, under the previous conditions, is characterized by a model of non-integer order. In fact, the PDE solution in the s - domain corresponds to the expression:

$$U(x,s) = \frac{U_0}{s} G(s), \quad G(s) = e^{-x\sqrt{\frac{s}{k}}} \tag{20}$$

where x is the space coordinate and U_0 is the boundary condition.

The corresponding solution in the time domain yields:

$$u(x,t) = U_0 erfc\left(\frac{x}{2\sqrt{kt}}\right) = U_0\left[1 - \frac{2}{\sqrt{\pi}} \int_0^{\frac{x}{2\sqrt{kt}}} e^{-u^2} du\right] \tag{21}$$

In our study we adopt the numerical integration based on the discrete approximation to differentiation, yielding the equation:

$$u[j+1,i] = (u[j,i+1] + u[j,i-1])r + (1-2r)u[j,i] \tag{22}$$

where $r = k\Delta t(\Delta x^2)^{-1}$, $\{\Delta x, \Delta t\}$ and $\{i, j\}$ are the increments and integration indices for space and time, respectively.

We verify that the results obtained through the numerical approach differ from the analytical results for low frequencies. This is illustrated in Figure 18, which depicts the polar diagram of $G(j\omega)$, for $x = 3.0$ m and $k = 0.042$ $m^2 s^{-1}$, both for the theoretical and numerical methods.

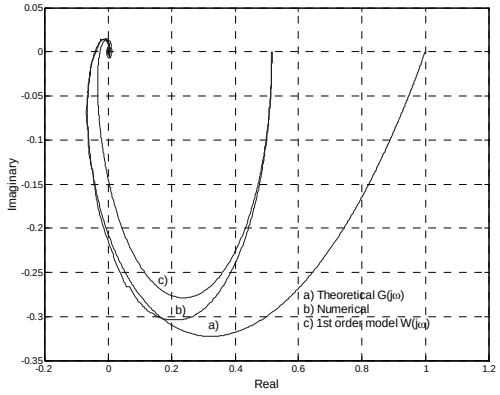

Figure 18- Nyquist diagram of $G(j\omega)$ for $x = 3.0$ and $k = 0.042\text{m}^2\text{s}^{-1}$.

It is clear that the chart has similarities to those of systems with time-delay. In this line of thought we consider the control of the heat system with two types of algorithms. In a first phase (Fig. 19 a) we adopt the simple *PID* controller ($G_c(s) = k_p\,[1+sT_d+(sT_i)^{-1}]$) tuned according with the Ziegler-Nichols open loop method. In this case the tuning heuristics leads to an approximate model $W(s) = k_B e^{-sT}/(s\tau + 1)$ with $k_B = 0.52$, $T = 0.165$, $\tau = 1.235$ and the *PID* parameters $k_p = 0.3484$, $T_d = 0.0825$ *s*, $T_i = 0.33$ *s*. Figure 20 depicts the step response of the closed-loop system for $R(s) = 1/s$ and $x = 3.0$ m.

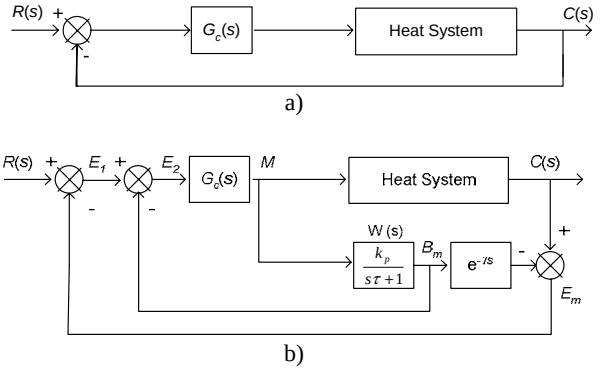

Figure 19 - Block diagram of closed-loop system with a) *PID* b) *PID* and Smith predictor.

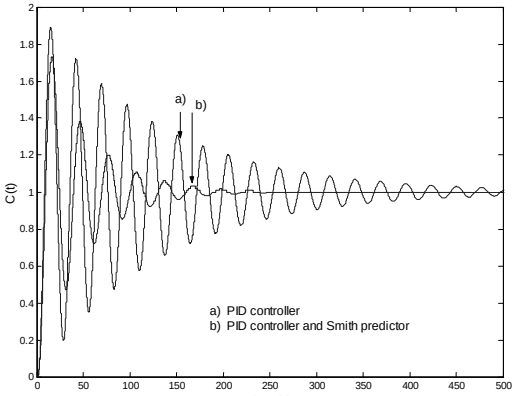

Figure 20 - Step response of closed-loop system for $k_p = 0.3484$, $T_d = 0.0825$ s and $T_i = 0.33$ s

In a second phase (Fig. 19 b), we adopt the previous *PID* controller but we apply the Smith predictor. This algorithm a well-known dead-time compensation technique that is very effective in improving the control of processes having time delays. Figure 20 shows the corresponding time response for $R(s) = 1/s$.

It is clear that the Smith predictor leads to a superior response, revealing that we can adopt with success classical control algorithms in fractional-order dynamical systems.

IV. CONCLUSIONS

This paper presented the fundamental aspects of the theory of FC, the main approximation methods for the fractional-order derivatives calculation and the implication of the FC concepts on the extension of the classical systems theory. Bearing these ideas in mind, several distinct systems were described and their dynamics was analyzed in the perspective of fractional calculus. It was shown that fractional-order models capture phenomena and properties that classical integer-order simply neglect. In this line of thought, this article is a step towards the development of systems modeling and control based on the theory of FC.

REFERENCES

[1] K. B. Oldham and J. Spanier, *The Fractional Calculus*, Academic Press, 1974.

[2] K. S. Miller and B. Ross, *An Introduction to the Fractional Calculus and Fractional Differential Equations*, John Wiley and Sons, 1993.

[3] I. Podlubny, *Fractional Differential Equations*, Academic Press, San Diego, 1999.

[4] A. Oustaloup, *La Commande CRONE: Commande Robuste d'Ordre Non Entier*, Hermes, Paris, 1991.

[5] J. T. Machado, "Analysis and Design of Fractional-Order Digital Control Systems", in *SAMS Journal Systems Analysis, Modelling, Simulation*, vol. 27, 1997, pp. 107–122.

[6] Ramiro S. Barbosa, J. A. T. Machado and Isabel M. Ferreira, "A Fractional Calculus Perspective of PID Tuning", Proc. of the ASME Int. 19th Biennial Conf. on Mechanical Vibration and Noise, September, 2003, Chicago, Illinois, USA.

[7] M. F. Silva, J. A. T. Machado and A. M. Lopes, "Comparison of fractional and integer order control of an hexapod robot", Proc. of the ASME Int. 19th Biennial Conf. on Mechanical Vibration and Noise, September, 2003, Chicago, Illinois, USA.

[8] L. Figueiredo, J. Machado and J. Ferreira, "Simulation and Dynamical Analysis of Freeway Traffic", Proc. IEEE Int. Conf. on Systems, Man and Cybernetics, October 2003, Washington D.C., pp. 3607-3612.

[9] Jean-Luc Battaglia, Ludivic Le Ly, J. Batsale, A. Oustaloup and O. Cois, "Utilisation de Modèles d´identification non entiers pour la Résolution de problèmes inverses en Conduction", *Int. Journal Therm. Science*, vol. 39, 2000, pp. 374–389.